Holographic axilens: high resolution and long focal depth

N. Davidson, A. A. Friesem, and E. Hasman

Department of Electronics, Weizmann Institute of Science, Rehovot 76100, Israel

Received September 11, 1990; accepted January 31, 1991

We report a novel aspheric holographic optical element, the holographic axilens, for achieving extended focal depth while keeping high lateral resolution. The element is designed according to special optimization techniques and recorded as a computer-generated hologram. The results for a specific element, which has a depth of focus of 30 mm, a lateral resolution of 80 μm, a focal length of 1250 mm, and a diameter of 12.5 mm at a wavelength of 633 nm, are presented.

Optical elements that have long focal depth as well as high lateral resolution are needed for a variety of applications, including precision alignment and profile measurements. Conventional elements (spherical lenses, mirrors, etc.) cannot achieve these two goals simultaneously; high lateral resolution requires high numerical apertures, whereas long depth of focus requires low numerical apertures. Specifically, the combination of Abbe's formula for lateral resolution ($1/\delta x$) and Rayleigh's formula for the depth of focus δz yields[1]

$$\delta z = \frac{4(\delta x)^2}{\lambda}, \tag{1}$$

where λ is the wavelength of the light. Possible approaches to improve this situation include apodization and digital restoration.[2] These approaches result in some loss of energy or involve a complicated optical system or must incorporate digital computers. Another approach uses an axicon,[3] a conical optical element that may have an arbitrarily long depth of focus while still maintaining a high lateral resolution; the axicon has recently been suggested as an element that can produce a nearly nondiffracting beam.[4] Unfortunately, the axicon concentrates only a small fraction of the energy into the focused beam, which results in an extremely low light efficiency.

In this Letter we present a special aspheric holographic optical element that can have arbitrarily long focal depth as well as high lateral resolution. This element essentially combines the properties of the long focal depth of an axicon and the high energy concentration of a conventional spherical lens and is, therefore, named an axilens. We derive the phase function for a specific axilens, record it as a computer-generated hologram, and then verify the numerical simulations experimentally.

A spherical holographic lens adds a spherical phase to an incoming monochromatic wave front with a wavelength λ of the form

$$\phi(r) = \frac{2\pi}{\lambda}\sqrt{r^2 + f^2}, \tag{2}$$

where r is the radial coordinate and f is the focal length of the holographic lens. By resorting to the paraxial case, the spherical phase may be approximated by a quadratic term

$$\phi(r) = \frac{2\pi}{\lambda}\frac{r^2}{2f}, \tag{3}$$

where a constant term was omitted. Such a lens focuses the incoming wave to an Airy pattern,[5] with approximately 84% of the energy contained within a central peak of width equal to $2.44\lambda F_{\#}$, where $F_{\#} = f/2R$ and R is the radius of the hologram. The depth of focus is proportional to $\lambda F_{\#}^2$, where the proportionality constant depends on the exact definition used for the focal depth,[5] but is typically approximately one. If, instead of a constant focal length f, the holographic lens would be composed of zones each having a different focal length, the depth of focus would increase. By choosing these zones to be concentric rings with an infinitesimal width, we can express the lens phase function as

$$\phi(r) = \frac{2\pi}{\lambda}\frac{r^2}{2f(r)}, \tag{4}$$

where $f(r)$ is a continuous function instead of a constant. The simplest nonconstant function that can be used is a linear function $f(r) = ar$, where a is a constant. Insertion of this linear function into Eq. (4) yields exactly the phase function of an axicon,[3]

$$\phi(r) = \frac{\pi}{\lambda}\frac{r}{a}. \tag{5}$$

The focal range along the z axis of such an axicon is $0 < z < aR$. The width of the central peak is approximately $a\lambda$, and the fraction of the energy that the peak contains is approximately $a\ \lambda/R$, which is typically a very small number.

A more general form for the variable focal length $f(r)$ may be the following monotonic function:

$$f(r) = f_0 + ar^b, \tag{6}$$

where a, b, and f_0 are constants. For a positive constant a, the geometrical-optics prediction of the focal range for an element with the focal length of Eq. (6) will be $f_0 < z < f_0 + aR^b$, which leads to a focal depth δz_g of aR^b. The geometrical parameters and the distribution of rays for such an axilens are shown in Fig. 1.

0146-9592/91/070523-03$5.00/0

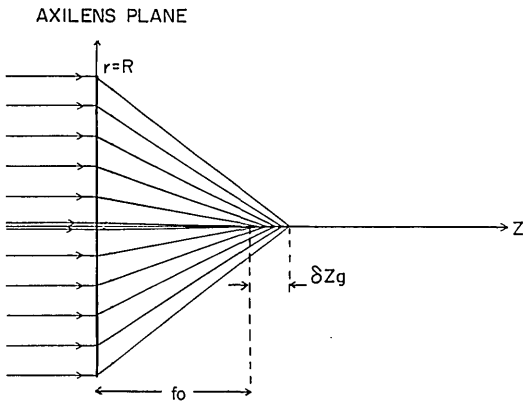

Fig. 1. Geometrical parameters and schematic distribution of rays with an input plane wave focused by an axilens.

The constant b depends on the desired intensity distribution of the central peak. For example, if we require that the central peak throughout the focal range have uniform intensity, then the area of each ring having a focal distance between f and $f + \delta f$ should be the same. Since the area of such a ring is $r\delta r$, we can express this requirement as

$$\delta f(r) = 2ar\delta r. \tag{7}$$

Integration of Eq. (7) on both sides yields

$$f(r) = f_0 + ar^2. \tag{8}$$

Equation (8) indicates that the requirement for uniform intensity distribution of the peak results in $b = 2$. Note that Eq. (7) will differ for other intensity distributions of the central peak in the focal range, and consequently b will be different. The constant a in Eq. (6) can be expressed in terms of the desired focal depth of the element as

$$a = \frac{\delta z_g}{R^2}. \tag{9}$$

Finally, by substitution of Eqs. (8) and (9) into Eq. (4), the phase function of the axilens can be written as

$$\phi(r) = \frac{\pi}{\lambda} \frac{r^2}{f_0 + \frac{\delta z_g}{R^2} r^2}. \tag{10}$$

The parameters f_0 and R in Eq. (10) can be chosen according to a specific application for the axilens.

We performed numerical simulations and initial experiments to verify the above geometrical-optics predictions for the depth of focus. We used a hologram with a phase function of Eq. (10) that is illuminated with a unit-amplitude plane wave. For the simulation we calculated the intensity distribution at any plane along the z axis by solving numerically the Fresnel diffraction integral,[5]

$$I(z, r) = \left(\frac{2\pi}{\lambda z}\right)^2 \left| \int_0^R \exp\{i2\pi[r'^2/2\lambda z - \phi(r')]\} \times J_0(2\pi r r'/\lambda z) r' \mathrm{d}r' \right|^2, \tag{11}$$

where r denotes the radial position at the plane and J_0 is the zero-order Bessel function. The results for an axilens with the parameters $\lambda = 633$ nm, $R = 12.5$ mm, $f_0 = 1220$ mm, and $\delta z_g = 29$ mm are presented in Figs. 2 and 3; these parameters were chosen to illustrate extended focal depth and yet reasonable energy concentration in the focused beam.

Figure 2 shows the intensity distribution along the z axis $I(z, r = 0)$, in the focal range of the axilens. For comparison, we also present the corresponding distribution for a spherical holographic lens that has the same aperture and a focal distance of 1250 mm. As is evident, the depth of focus, over which the intensity along the axis is constant, is approximately three times greater for this axilens than for the spherical lens. As expected, the peak intensity is lower for the axilens by approximately the same factor. Indeed, in general, we found that as the focal depth is increased, the peak intensity decreases by the same factor. It is interesting to note that the focal range has shifted by approximately 15 mm in comparison with the geometrical-optics prediction; it now begins at a distance of ap-

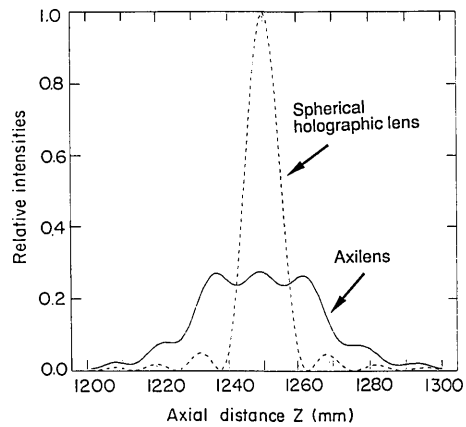

Fig. 2. Calculated intensity distribution as a function of the axial distance around the focal region for the axilens and a spherical holographic lens.

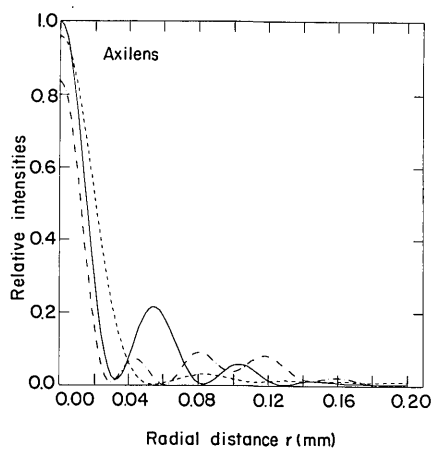

Fig. 3. Calculated intensity distribution at different distances z from the axilens: dashed curve, $z = 1235$ mm; solid curve, $z = 1250$ mm; dashed–dotted curve, $z = 1265$ mm.

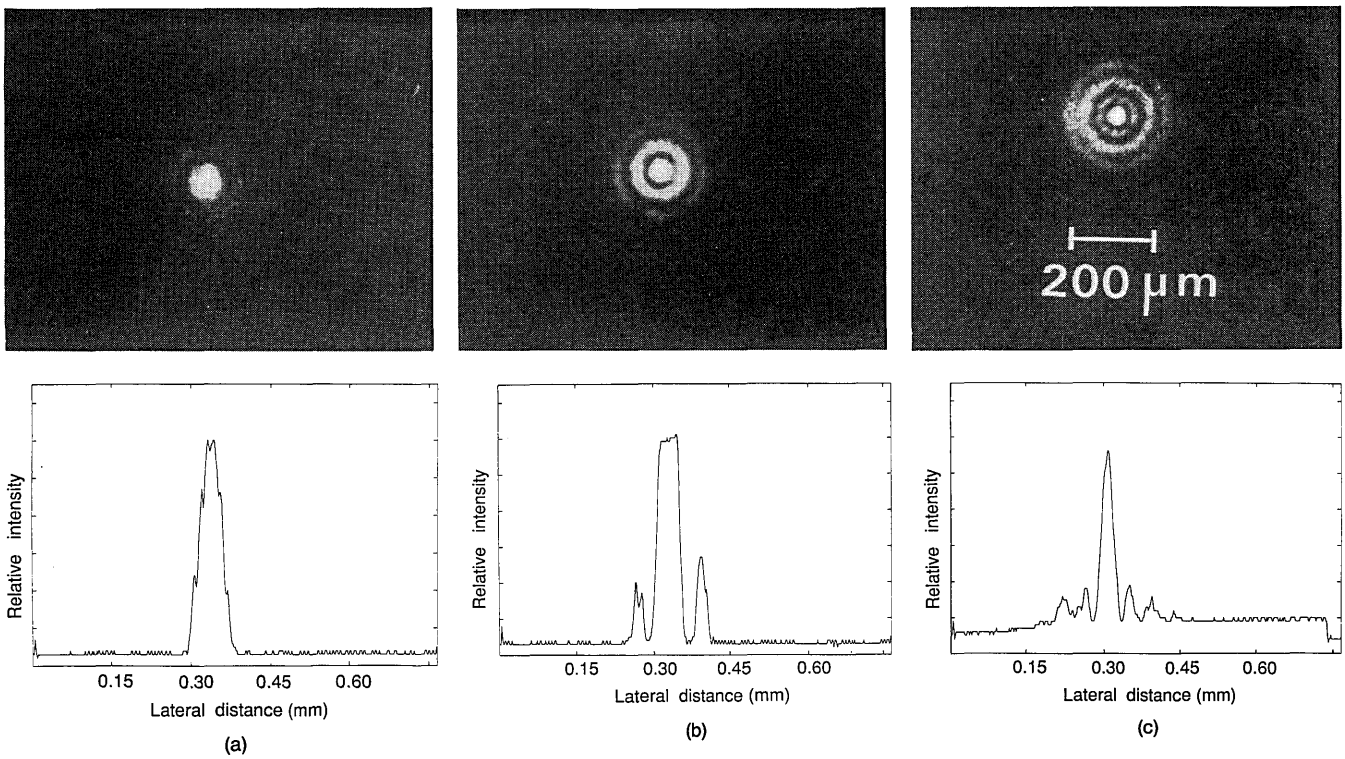

Fig. 4. Photographs of the focused spots (top) and the intensity cross sections (bottom) at several distances from the axilens: (a) $z = 1235$ mm, (b) $z = 1250$ mm, (c) $z = 1265$ mm.

proximately 1235 mm instead of 1220 mm from the axilens. This shift may be attributed to unequal interference effects along the z axis.

To determine the exact intensity distribution at a certain distance from the axilens, we solved Eq. (11) at three different distances from the lens. The results, shown in Fig. 3, give the intensity distribution as a function of radial distance for $z = 1235$ mm, $z = 1250$ mm, and $z = 1265$ mm. As is evident, the intensity distribution of the central lobe for the axilens remains close to the diffraction-limited spot size of $2.44\lambda F_{\#} \approx 80$ μm. Note that the sidelobes for the intensity distribution of the axilens are higher than for an Airy pattern that would be obtained with a spherical lens; consequently, the energy in the central lobe is reduced, typically by the same factor as the peak intensity.

For the experiment the axilens was recorded as a binary computer-generated hologram.[6] In order to separate the diffraction orders, a linear phase term of $2\pi x \sin\theta_x/\lambda$ was added to the axilens phase function of Eq. (10). The off-axis angle θ_x was chosen as 0.05 rad, and x is one of the transverse coordinates. The axilens was then illuminated with a uniform plane wave derived from a He–Ne laser of $\lambda = 633$ nm, and the intensity distribution was detected at three different distances that correspond to those chosen in the simulation. The results are presented in Fig. 4, which shows photographs of the focused spots as well as cross-sectional traces that were directly detected with a charge-coupled-device array. The intensity distribution is shown at $z = 1235$ mm [Fig. 4(a)], $z = 1250$ mm [Fig. 4(b)], and $z = 1265$ mm [Fig. 4(c)]. By comparison of these experimental results with the numerical results of Fig. 3, it is evident that good agreement exists; some difference in the sidelobe levels may be attributed to thickness variations of the recording plate.

We conclude by noting that it is possible to increase the focal depth of the axilens even further, but with a corresponding reduction in intensity along the lens axis. Moreover, the approach is also valid for small-$F_{\#}$ axilenses, but there the paraxial approximation of Eq. (3) may no longer be valid, and Eq. (2) must be used directly.

References

1. G. Bickel, G. Hausler, and M. Maul, Opt. Eng. **24**, 975 (1985).
2. J. Ojeda-Castaneda, R. Ramos, and A. Noyola Isgleas, Appl. Opt. **27**, 2583 (1988).
3. J. H. Mcleod, J. Opt. Soc. Am. **44**, 592 (1954).
4. A. Vasara, J. Turunen, and A. T. Friberg, J. Opt. Soc. Am. A **6**, 1748 (1989).
5. J. W. Goodman *Introduction to Fourier Optics* (McGraw-Hill, New York, 1968), p. 64.
6. G. J. Swanson and W. B. Veldkamp, Opt. Eng. **28**, 605 (1989).